

# SCIENTIFIC REPORTS

OPEN

## Curvature-enhanced Spin-orbit Coupling and Spinterface Effect in Fullerene-based Spin Valves

Shiheng Liang<sup>1,\*</sup>, Rugang Geng<sup>1,\*</sup>, Baishun Yang<sup>2</sup>, Wenbo Zhao<sup>3</sup>, Ram Chandra Subedi<sup>1</sup>, Xiaoguang Li<sup>3</sup>, Xiufeng Han<sup>2</sup> & Tho Duc Nguyen<sup>1</sup>

Received: 26 June 2015

Accepted: 09 December 2015

Published: 20 January 2016

We investigated curvature-enhanced spin-orbit coupling (SOC) and spinterface effect in carbon-based organic spin valves (OSVs) using buckyball  $C_{60}$  and  $C_{70}$  molecules. Since the naturally abundant  $^{12}C$  has spinless nuclear, the materials have negligible hyperfine interaction (HFI) and the same intrinsic SOC, but different curvature SOC due to their distinct curvatures. We fitted the thickness dependence of magnetoresistance (MR) in OSVs at various temperatures using the modified Jullière equation. We found that the spin diffusion length in the  $C_{70}$  film is above 120 nm, clearly longer than that in  $C_{60}$  film at all temperatures. The effective SOC ratio of the  $C_{70}$  film to the  $C_{60}$  film was estimated to be about 0.8. This was confirmed by the magneto-electroluminescence (MEL) measurement in fullerene-based light emitting diodes (LED). Next, the effective spin polarization in  $C_{70}$ -based OSVs is smaller than that in  $C_{60}$ -based OSVs implying that they have different spinterface effect. First principle calculation study shows that the spin polarization of the  $dz^2$  orbital electrons of Co atoms contacted with  $C_{60}$  is larger causing better effective spin polarization at the interface.

Organic semiconductor (OSEC) has recently attracted great attention in the spintronics community since it possesses a long spin lifetime due to the reduced intrinsic spin-orbit coupling (SOC) caused by the light-weight elements, and relatively weak hyperfine interaction (HFI) associated with the symmetry of the  $\pi$ -electron orbital<sup>1,2</sup>. Therefore OSECs with high carrier mobility would show spin coherence that may be maintained over macroscopic distances. The motivation for searching materials with long spin diffusion length is to obtain large magnetoresistance (MR) in organic spin valves (OSVs)<sup>3–5</sup>, high performance of spin-polarized organic light emitting diodes<sup>6–9</sup> and the realization of electrically-controlled spin-transport polarization devices such as spin-transistors<sup>10</sup>. An OSV consists of a thin layer of organic molecules or polymers sandwiched between two ferromagnetic (FM) contacts (see Fig. 1a); the resistance of the device depends on the relative magnetization configuration of the electrodes. The operation of the OSV would include spin injection and detection by magnetic electrodes, and spin transport accompanied by the spin relaxation in the organic interlayer; the former is related to the interfacial spin-polarization, dubbed spinterface<sup>11–17</sup> which is influenced by the spin polarization of the FM electrode and the OSEC/electrode orbital hybridization, whereas the latter depends on spin relaxation time and charge diffusion coefficient in the organic spacer which defines the spin diffusion length of the material (see Fig. 1b).

So far, there exist several challenges on understanding spin loss mechanism and temperature dependence of spin diffusion length in OSECs<sup>18</sup>. Drew *et al.*<sup>19</sup> using muon-spin spectroscopy found that the carrier spin diffusion length in an  $Alq_3$  molecule-based OSV is significantly quenched at a temperature above 100 K leading to unobservable MR at the higher temperature. In contrast, using the ferromagnetic resonance spin pumping technique Jiang *et al.* found the temperature independence of spin diffusion length in  $Alq_3$  film<sup>20</sup>. In addition, Kawasugi *et al.*<sup>21</sup> recently found ~10% MR in a TPD-based OSV at all temperatures. Although the spin diffusion length was not measured, the result implies that spin diffusion length in TPD molecules is also insensitive with the device temperature. Also, it has been theoretically and experimentally demonstrated that the HFI plays a crucial role in

<sup>1</sup>Physics and Astronomy Department, University of Georgia, Athens, Georgia 30602, USA. <sup>2</sup>State Key Laboratory of Magnetism, Beijing National Laboratory for Condensed Matter Physics, Institute of Physics, Chinese Academy of Sciences, Beijing 100190, China. <sup>3</sup>Hefei National Laboratory for Physical Sciences at Microscale, Department of Physics, University of Science and Technology of China, Hefei 230026, and Collaborative Innovation Center of Advanced Microstructures, Nanjing University, Nanjing 210093, China. \*These authors contributed equally to this work. Correspondence and requests for materials should be addressed to T.D.N. (email: ngtho@uga.edu)

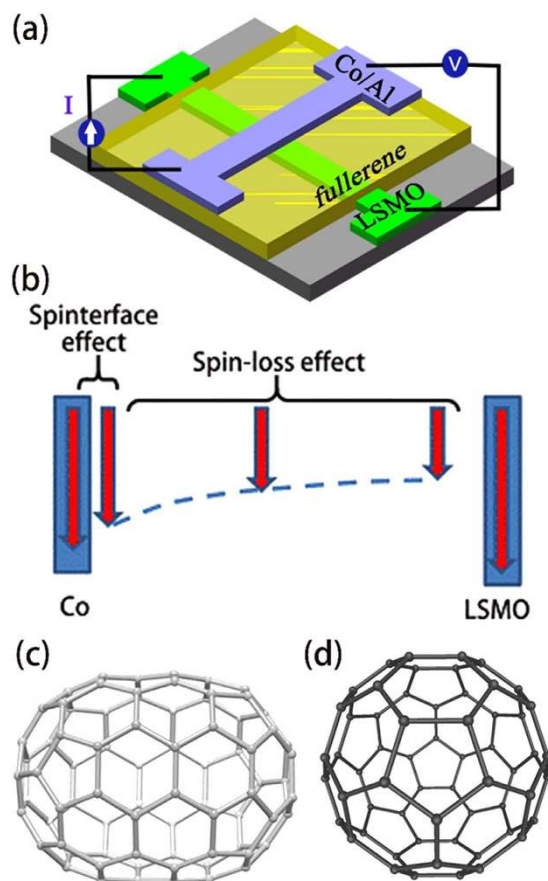


**Figure 1.** (a) Schematic representation of a typical device that consists of two FM electrodes and an OSEC spacer. An in-plane magnetic field,  $B$ , is swept to switch the magnetization directions of the two FM electrodes separately while the device resistance is measured using the four probe measurement technique. (b) The schematic representation of spinterface effect and spin-loss effect in organic spin valves. The arrows show the spin polarization of electrodes and transport electrons. Molecular structures of fullerene (c)  $C_{70}$  and (d)  $C_{60}$ .

all spin responses in PPV-based polymers<sup>5,22,23</sup>. However, Ando *et al.*<sup>24</sup> recently showed that a pure spin current can be pumped from a ferromagnetic electrode into conducting polymers and can be detected using inverse spin Hall effect, where intrinsic SOC plays an important role. The study calls for the reconsideration of the role of SOC on the spin transport in OSECs even when the material does not contain heavy metal<sup>24,25</sup>. However, there is a limitation in their experimental technique: the presence of a large magnetic field during the measurement quenches the HFI leading to an extremely long spin diffusion length of greater than 200 nm at room temperature<sup>26</sup>. So far, there is very little effort to understand the effect of intrinsic SOC in conventional OSEC-based spin valves. Nevertheless, there are several studies of spin response in metal complex molecules where large intrinsic SOC from heavy metals is clearly dominant over other spin interaction mechanisms<sup>27</sup>. The effective way, we believe, to remove the strong effect of HFI thereby considering only SOC effect is to study fullerene-based spin valves<sup>28–33</sup>; the materials are composed of 99% naturally abundant <sup>12</sup>C atoms that have spinless nuclei, and thus zero HFI. Since the intrinsic SOC in  $C_{60}$  is estimated about 10 mK, the fullerene is assumed to have a long spin relaxation time<sup>34</sup>. In addition,  $C_{60}$ -based spin valves show relatively large magneto-resistance (MR) at room temperature<sup>30–32</sup>, which is promising for the organics-based spintronics applications. In contrast to conventional OSECs,  $C_{60}$  material shows its mechanical robustness against the metal penetration during the electrode fabrication<sup>32,35</sup> and therefore is an ideal material to study *spinterface science*. However, various  $C_{60}$ -based OSVs studies surprisingly show that the spin diffusion length in  $C_{60}$  varies from 10 nm to more than 100 nm, not significantly larger than in conventional OSECs<sup>29,30,33</sup>. It is still not clear whether there exist any other spin loss mechanisms other than intrinsic SOC in fullerene. Recently, the study of SOC strength in carbon-based materials such as graphene, carbon nanotube and fullerene has gained tremendous attention due to their non-trivial topological phase that induces a charge hopping between the orbitals in the  $\pi$  and  $\sigma$  bands between neighboring carbon atoms causing the so-called curvature SOC<sup>34,36–38</sup>. Perhaps,  $C_{60}$  and  $C_{70}$  fullerenes with quite distinctive topological phases (see Fig. 1c,d) may be the most sufficient choice for comparing the effect of curvature SOC on spin transport. *Such critical study in fact has not been empirically achieved yet in fullerene-based spin valves*. Nevertheless, Arbogast *et al.*<sup>39</sup> firmly reported the stronger SOC in  $C_{60}$  compared to  $C_{70}$  molecules while studying their photophysical properties. In contrast, various electron paramagnetic resonance studies on the doped  $C_{60}$  and  $C_{70}$  either in solution or in solid forms show that their relative electron  $g$  value depends on the use of doping agents<sup>40,41</sup>.

In this paper, we systematically studied the spin diffusion length of  $C_{60}$  and  $C_{70}$  films and the spinterface effect by using MR response in fullerene-based spin valves. The buckyballs,  $C_{70}$  and  $C_{60}$ , possess the same intrinsic SOC but might have different effective SOC strength caused by their different curved structures. We found that a spin diffusion length of  $C_{70}$  is above 120 nm, inevitably longer than that of  $C_{60}$  at all temperatures, presuming that the effective SOC in  $C_{70}$  is smaller. The difference in effective SOC strength between the fullerenes can be confirmed by the magneto-electroluminescence (MEL) study in fullerene-based light emitting diodes (LED) where the  $C_{60}$  MEL response shows wider width (implying stronger SOC strength) than  $C_{70}$  MEL response<sup>3,42,43</sup>. In addition, the effective spin polarization of the electrodes in the  $C_{60}$ -based device is also larger. However, they share the same reduction trend with increasing temperature. The discrepancies can be explained by the structural difference between the molecules causing (i) different effective SOC strength, and (ii) the different electron orbital hybridization between the molecules and the ferromagnetic electrodes. The latter is verified by the density functional theory (DFT) calculation.

## Results & Discussion

Figure 1a shows the OSV schematic representation of the devices used in this study where a 50 nm  $\text{La}_{0.67}\text{Sr}_{0.33}\text{MnO}_3$  (LSMO) film with ~100% spin polarization at low temperature is used as the bottom electrode and a 15 nm Co film with ~30% spin polarization is used as the top electrode<sup>3</sup>. It is possible to switch the relative magnetization of the ferromagnetic electrodes between parallel (P) and anti-parallel (AP) alignments, upon sweeping the external magnetic field,  $B$ . The device resistance  $R(B)$  at the field of  $B$ , is then dependent on the relative magnetization orientations. The MR response is commonly defined as:  $\text{MR} = [R(B) - R(P)]/R(P)$ , where  $R(P)$  is the device resistance for the parallel magnetization configuration. Figure 1c,d show the chemical structures of  $C_{60}$  and  $C_{70}$ . A  $C_{60}$  molecule has a spherical cage-like fused-ring structure with radius of 7.1 Å while a  $C_{70}$  molecule has a belt of 6 hexagons inserted in at the equator of a  $C_{60}$  molecule, resulting in an ellipsoid with short and long axes of 7.12 Å and 7.96 Å, respectively<sup>44,45</sup>. Therefore the  $C_{60}$  molecule has larger symmetry and curvature than the  $C_{70}$  molecule. We note that the fullerene films mostly show amorphous phase with an excellent surface roughness (see Fig. S1).

Figure 2a,b show the MR loops of LSMO/ $C_{60}$ (120nm)/Co/Al and LSMO/ $C_{70}$ (120 nm)/Co/Al OSV devices measured at 20 K under an applied bias voltage of  $-20$  mV, respectively. The background of all MR response (non-spin valve MR) caused by magnetic anisotropy of the electrodes is subtracted (see Fig. S2c,d for the original MR response)<sup>46,47</sup>. The IV characteristics at 20 K are shown in Fig. S2a. The red (black) curve denotes MR measurement while decreasing (increasing) magnetic field. The insets show the relative electrode magnetizations upon sweeping from positive  $B$ . The MR of the  $C_{70}$ -based OSV is  $-9.0\%$  while the MR of the  $C_{60}$ -based OSV is  $-13.3\%$ . The MR response in general follows the magnetic coercive field of the electrodes. Figure 2c shows the MR of LSMO/fullerene(180 nm)/Co OSVs device versus temperature. The MR decreases when temperature increases for both  $C_{60}$ - and  $C_{70}$ -based OSVs. This behavior is generic for all OSVs using the LSMO electrode<sup>3,5,48,49</sup>. However, the MR magnitude of  $C_{60}$  at this thickness is consistently larger than that of  $C_{70}$  at all temperatures at this fullerene thickness. The reduction of MR at higher temperature in general can be understood by the reduction of LSMO spin polarization and/or fullerene spin diffusion length.

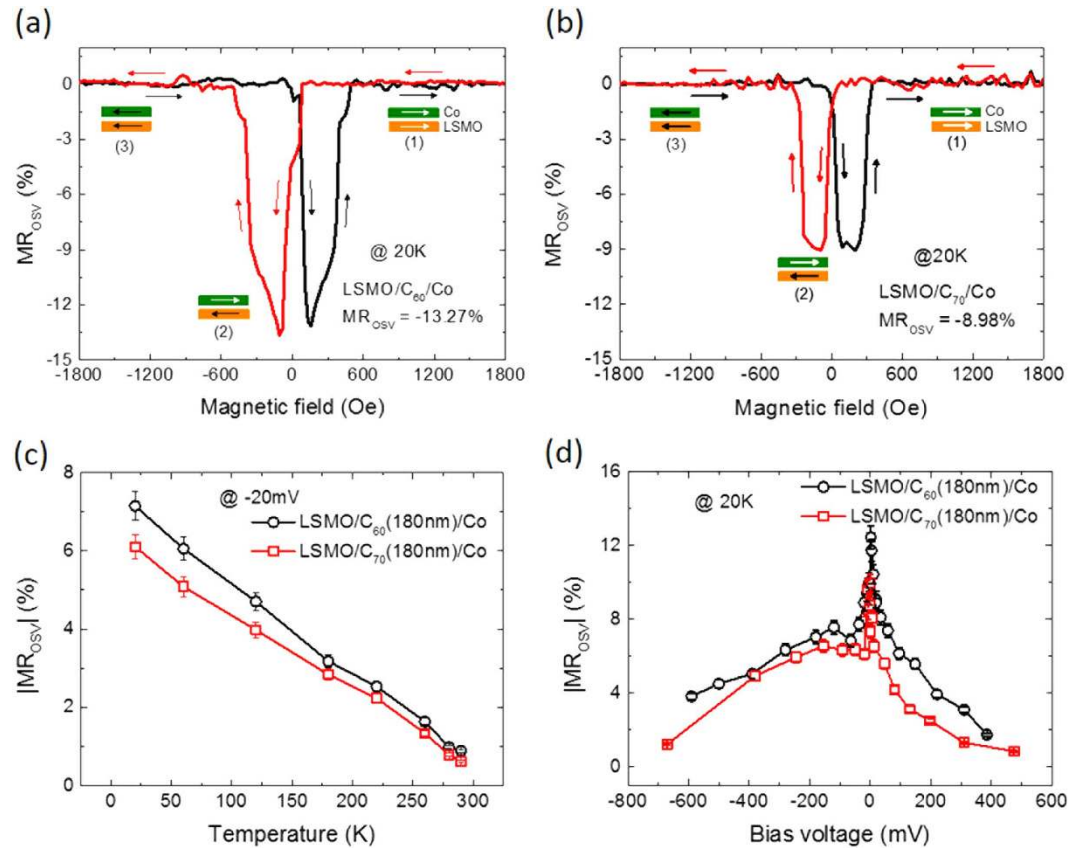
Figure 2d shows the bias voltage dependence of MR. Firstly, the MR decreases with the increase in the junction voltage. There are two possible explanations for the bias-voltage dependence behavior for the reduction of MR at high bias voltages: (i) The Fermi energy which decides the density of state of injection spin polarization might be shifted under a relatively large applied bias voltage; therefore the effective spin polarization of LSMO ( $P_1$ ) and/or Co ( $P_2$ ) might be modified<sup>48</sup>; (ii) Since the two-step tunneling of electron from the ferromagnetic electrode into the fullerene interlayer favorably happened at large bias voltages does not conserve spin, the effective spin polarization of the electrode is smaller at larger bias voltage<sup>5,50</sup>. The asymmetry MR behavior versus applied voltage in our studies has been commonly observed by many groups<sup>3,48,51</sup>.

Figure 3a shows the thickness dependent MR of  $C_{60}$ - (black dots) and  $C_{70}$ - (red dots) based OSVs at 120 K presented in the log scale, where the MR in  $C_{60}$ -based OSVs shows considerably stronger dependence than the MR in  $C_{70}$ -based OSVs. We found that the MR magnitude in the  $C_{70}$ -based OSVs is the largest at ~80 nm thickness (see Fig. S3a). Such behavior was previously reported in  $C_{60}$ -based OSVs probably due to the morphology effect rather than the ill-defined organic layer caused by the cobalt inclusion<sup>32,33,35</sup>. The MR magnitude of fullerene-based OSVs gets smaller at the larger fullerene spacer thickness,  $d$ . We note that the ill-defined fullerene layer was found to be less than 15 nm (see Fig. S5). The smaller MR magnitude found in the larger spacer thickness can be explained by the reduction of the spin polarization of the injected carriers when travelling across the interlayer. Indeed, the MR magnitude in OSVs is normally described by the modified Jullière model<sup>3</sup>:

$$\frac{\Delta R}{R} = \frac{2P_1 \cdot P_2 \cdot \exp(-d/L_S)}{1 - P_1 \cdot P_2 \cdot \exp(-d/L_S)} \quad (1)$$

where  $P_1$  and  $P_2$  are the effective spin polarization at the interface of the magnetic electrodes;  $L_S$  is the spin diffusion length of the spacer.

In Fig. 3a, the black and red lines are the fitting data at 120 K using Eq. 1, where  $P_1 \cdot P_2$  and  $L_S$  are the fitting parameters. For  $C_{70}$ -based OSVs,  $|P_1 \cdot P_2| = (0.09 \pm 0.01)$  and  $L_S = (123 \text{ nm} \pm 13 \text{ nm})$  while for  $C_{60}$ -based OSVs,  $|P_1 \cdot P_2| = (0.16 \pm 0.03)$  and  $L_S = (86 \text{ nm} \pm 8 \text{ nm})$ . We fitted the thickness dependent MR magnitude at different temperatures using the same method (see Figs S3 and S4 for details). We found that the spin diffusion length  $L_S$  of  $C_{70}$  is indeed larger than that of  $C_{60}$  at all temperatures (Fig. 3b). In contrast, the effective spin polarization,  $|P_1 \cdot P_2|$ , of  $C_{70}$  is always smaller than that in  $C_{60}$  (see Fig. 3c,d). It should be noticed that  $L_S$  of fullerene weakly depends on temperature, in contrast to  $L_S$  in the  $\text{Alq}_3$  film reported by Drew *et al.*<sup>19</sup>, which decays quickly and is vanished at temperature higher than 100 K. We compare  $|P_1 \cdot P_2|$  with the magnetization near the surface of LSMO electrode



**Figure 2.** The magneto-resistance response of the spin-valve devices. MR loops of (a) LSMO(50 nm)/C<sub>60</sub>(120 nm)/Co(15 nm) and (b) LSMO(50 nm)/C<sub>70</sub>(120 nm)/Co(15 nm) OSV device measured at 20 K, with an applied bias voltage of −20 mV. The magnetization configurations are shown in the insets when the field is swept from positive field to negative field. (c) Temperature dependence of MR for the device of LSMO(50 nm)/C<sub>60</sub>(180 nm)/Co(15 nm) and LSMO(50 nm)/C<sub>70</sub>(180 nm)/Co(15 nm) OSV; (d) Bias voltage dependence of MR for the device of LSMO(50 nm)/C<sub>60</sub>(180 nm)/Co(15 nm) and LSMO(50 nm)/C<sub>70</sub>(180 nm)/Co(15 nm) OSV measured at 20 K. The bars in (c,d) show errors of the measurement.

measured by magneto-optical Kerr effect (MOKE)<sup>3</sup>. The insets of Fig. 3c,d show that the normalized effective spin polarization ( $P = |P_1 \cdot P_2|$ ) and LSMO magnetization follow a similar temperature dependence except at 120 K. This indicates that the LSMO spin polarization might be a culprit for the MR reduction at high temperature. This is in agreement with the recent results reported by Kawasugi *et al.*<sup>21</sup> who found that the MR was insensitive with the device temperature when the LSMO is replaced by the Co<sub>2</sub>MnSi heusler alloy. The obtained large spin diffusion length in fullerene-based OSVs at high temperature is similar to the value reported by Zhang *et al.*<sup>30</sup> at room temperature. In the following sections, we explain the differences of spin diffusion length  $L_S$  and effective spin polarization  $|P_1 \cdot P_2|$  between C<sub>70</sub> and C<sub>60</sub> molecules.

In OSECs, since charge hopping is the main conduction mechanism, the spin diffusion length is generally described by the relation:  $L_S = (D \cdot \tau_S)^{1/2}$ , where  $D$  is the carrier diffusion coefficient which is proportional to film mobility, and  $\tau_S$  is the spin relaxation time<sup>9</sup>. Since the C<sub>70</sub> has smaller mobility<sup>52</sup> but larger measured spin diffusion length, its spin relaxation time must be longer than that in C<sub>60</sub> leading to weaker SOC. Yu<sup>23</sup> theoretically found that in conventional OSEC where HFI is dominant,  $L_S$  is linear with  $D$  and thereby depending on the material mobility. However, in the material such as fullerene where SOC is the dominant interaction, the  $L_S$  is given by<sup>53</sup>:

$$L_S = \frac{R}{4\xi} \quad (2)$$

where  $R$  is the electron hopping distance, and  $\xi = \xi_{in} + \xi_{curv} + \xi_{Rashba}$  is the effective SOC strength where  $\xi_{in}$ ,  $\xi_{curv}$  and  $\xi_{Rashba}$  are the intrinsic, curvature and Rashba SOC, respectively. The small electric field in the measurement leads to a negligible  $\xi_{Rashba}$ <sup>34</sup>. For the close-packed structures of C<sub>70</sub> and C<sub>60</sub>, the nearest-neighbor distances between the adjacent molecules are  $\sim 10.1$  Å and  $\sim 10.04$  Å respectively<sup>54</sup>. This implies that the charge hopping distances are very similar in the materials. Equation 2 indicates that the spin diffusion length does not depend on the fullerene mobility. If the spin-related interaction contains only intrinsic SOC of carbon, the difference of spin diffusion length between C<sub>60</sub> and C<sub>70</sub> is simply the difference between the charge hopping distances. Figure 3b clearly shows that this is not the case and their effective SOC must contain the curvature-based SOC. From Eq. 2, the relative effective SOC strength between C<sub>60</sub> and C<sub>70</sub> molecules can be estimated as:



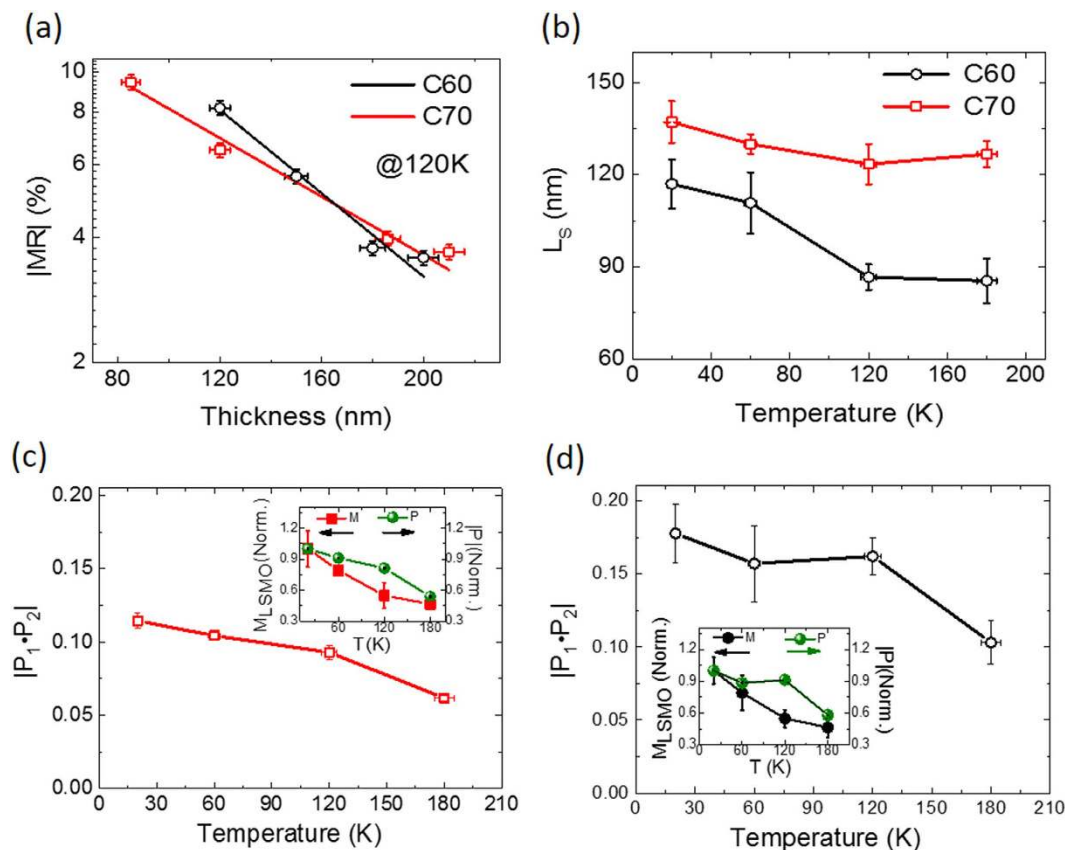


**Figure 3.** (a) Fullerene thickness dependence of MR at 120 K. The black and red open dots are measured MR of LSMO(50 nm)/C<sub>60</sub>/Co(15 nm) and LSMO(50 nm)/C<sub>70</sub>/Co(15 nm) OSVs, respectively. All MRs were taken at the junction voltage of −20 mV. The lines were fitted based on Eq. 1. (b) Temperature dependence of spin diffusion length,  $L_s$ , of C<sub>70</sub>- and C<sub>60</sub>-based OSVs. The spin polarization,  $|P_1 \cdot P_2|$ , of (c) C<sub>70</sub>- and (d) C<sub>60</sub>-based OSVs. The insets show the normalized  $|P_1 \cdot P_2|$ , and LSMO magnetization versus temperature. The bars show errors of the measurement and fittings.

$$\frac{\xi(C_{70})}{\xi(C_{60})} \approx \frac{L_s(C_{60})}{L_s(C_{70})} \quad (3)$$

From Eq. 3 and spin diffusion lengths in Fig. 3b, the relative SOC strength between C<sub>60</sub> and C<sub>70</sub> at various temperatures is calculated. Figure 4a shows that the effective SOC in C<sub>70</sub> is smaller than that in C<sub>60</sub> at all temperatures. Surprisingly, this ratio is slightly smaller at higher temperature. This might be related to their different orientational orders at different temperature<sup>55,56</sup>. Due to its higher symmetry, C<sub>60</sub> might be easily rotated at higher temperature in all directions; this might prolong the effective electron hopping distance in C<sub>60</sub> film, thereby reducing the spin diffusion length at high temperature. We note that our temperature dependence of  $L_s$  seems to conflict with Yu's theory, in which the charge hopping distance,  $R$  strongly depends on the temperature and is convergent to the nearest neighbor hopping above a certain temperature (80 K for Alq<sub>3</sub>)<sup>53</sup>. This suggests that either the hopping distance is already saturated to the nearest neighbor hopping in our studied temperature range or the theory needs to be adjusted. Recently, based on the new experimental evidence of spin precession missing in OSECs<sup>57,58</sup>, Yu suggested a new spin transport mechanism in organics utilizing the exchange-coupling between localized polarons, which can be much faster than polaron hopping. This spin-charge decoupling mechanism in principle can be used to explain the absence of the temperature dependent spin diffusion length described in the Fig. 3b since in contrast to hopping transport, the exchange coupling is insensitive with the temperature. This scenario was supported by recent experiment by Jiang *et al.*<sup>20</sup> where the spin precession of the pure spin current in Alq<sub>3</sub> film was absent and the spin diffusion length was found to be independent on the temperature. However, the spin diffusion length in exchange-coupling mechanism strongly depends on the carrier density. This seems to be contradicted to the relatively slower decay of MR with large junction bias observed by many group<sup>3,5,48</sup>. Our result on SOC of C<sub>60</sub> and C<sub>70</sub> is consistent with result reported by Arbogast *et al.*<sup>39</sup>, who studied photophysical properties of the C<sub>70</sub> compared to C<sub>60</sub> molecules. They found that the intersystem crossing rate between singlet and triplet manifolds in C<sub>60</sub> is larger than that in C<sub>70</sub>. This is a conclusive evidence that the SOC strength in C<sub>70</sub> is weaker than in C<sub>60</sub>.

In order to further strengthen our conclusion in the SOC strength of the fullerene, we performed the MEL measurement on ITO/PEDOT/fullerene(180 nm)/Ca/Al LEDs. The MEL response has been used to evaluate the

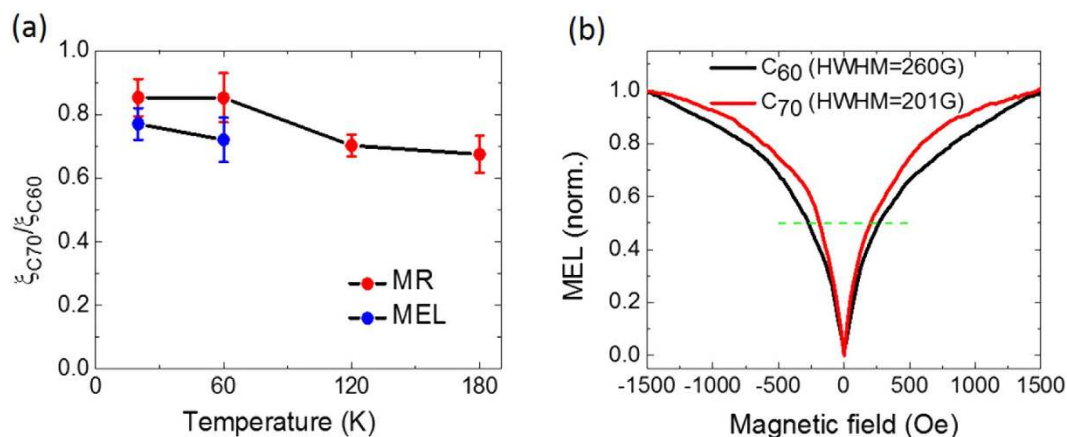


**Figure 4.** (a) Temperature dependence of relative SOC coupling strength between  $C_{60}$  and  $C_{70}$  molecules,  $\xi_{C70}/\xi_{C60}$  taken from MR in OSVs and MEL in LEDs. The bars show errors from the calculation. (b) Normalized magneto-electroluminescence (MEL) in fullerene LEDs at 20 K with the similar current density of about 1 mA/mm<sup>2</sup>. The line shows the half maximum of MEL.

electron-spin related interactions for the last several decades<sup>5,42,43</sup>. The device structure and IV characteristics are shown in the Fig. S6. Figure 4b clearly shows the MEL response of the  $C_{60}$ -based LED is broader than that of the  $C_{70}$ -based LED at 20 K. Ehrenfreund *et al.* theorized the magnetic field effect on the polaron pair spin mixing dynamics and hence electroluminescence under the presence of the spin-orbit interaction<sup>59</sup>. The SOC Hamiltonian included in the over all Hamiltonian can be written as:

$$H_{SO} = (\xi_{in} + \xi_{curv}) \mathbf{L} \cdot \mathbf{S} \quad (4)$$

where  $\mathbf{L}$ ,  $\mathbf{S}$  are the orbital and spin angular momentum operators.

The calculation shows that the half width at half maximum (HWHM) of the magnetic response scales with the effective SOC strength,  $\xi_{in} + \xi_{curv}$ . We estimate the effective SOC ratio of  $C_{70}$  over  $C_{60}$  is 0.77 which in agreement with the ratio shown in Fig. 4a. The MEL response at 60 K is shown in the Fig. S8 where much noisier MEL response were observed due to the weaker electroluminescence at higher temperature (Fig. S6). Nevertheless, the effective SOC ratio of about 0.7 is estimated. This is essentially in agreement with the study of SOC strengths by means of MR response in fullerene-based spin valves (Fig. 4a). At higher temperature, comparison is not conclusive due to the larger noise to signal ratio of the MEL response. We note that our result is in contrast to the recent theoretical calculation, in which the SOC caused by curvature in  $C_{60}$  is absent while the  $C_{70}$  has a large curvature SOC. The reason is that  $C_{70}$  molecule can be considered as a short nanotube capped by two semispheres that causes large curvature SOC in  $C_{70}$ <sup>34</sup>. We note that the difference cannot come from the polycrystallites of films since the films are mostly amorphous (see Fig. S1b). In fact, the much larger SOC than calculated value in carbon nanotubes found by Steele *et al.*<sup>36</sup> suggests that a considerable correction of theoretical calculations of curvature-based SOC should be done. The long spin diffusion length in fullerenes suggests that their effective SOC strength is weaker than the regular HFI strength in OSECs. This is in agreement with the long spin diffusion length obtained by Watanabe *et al.*<sup>25</sup> where the material only has intrinsic SOC since the HFI is quenched<sup>26</sup>.

Next, we show that the spinterface effect between fullerene and Co might play an important role in distinguishing the effective spin polarization between  $C_{60}$ - and  $C_{70}$ -based OSVs. To qualitatively understand the spinterface effect caused by the orbital hybridization at the interface, we performed the first-principle DFT calculations of the electron orbital absorption at the  $C_{60}/Co$  and  $C_{70}/Co$  interfaces where the ideal contact between the layer regardless of possible Co penetration was considered (see Figs S9 and 10, Supplementary Information for details). Figure 5a,b show the structure and charge density different isosurfaces of  $C_{60}$  on Co(111) respectively whereas Fig. 5c,d show the structure and charge density different isosurfaces of  $C_{70}$  on Co(111), respectively. The color bars describe the magnitude of charge density difference. The isovalue is set to  $\pm 0.05 \text{ \AA}^{-3}$ . The sensitivity of the  $dz^2$  states comes from the fact that this orbital has a lobe of electronic density oriented perpendicular to the Co surface. States deriving from the  $dz^2$  orbitals, which have long tails along the  $z$  direction, contribute significantly to the tunneling transport as compared to states deriving from other orbitals. Fig. 5e shows the spin polarization of the  $dz^2$  orbital electrons of the cobalt contacted with  $C_{70}$  (red) and  $C_{60}$  (black). The spin polarization of  $dz^2$  electrons of Co contacted with  $C_{60}$  is much larger than that of those contacted with  $C_{70}$  molecules. It means that the spinterface at the  $C_{60}/Co$  interface is better. The calculation indeed explains our experimental results at different spinterfaces namely  $C_{60}/Co$  and  $C_{70}/Co$ . We note that the workfunction of LSMO surface studied by photoemission spectroscopy was found to be sensitive to the organic solvents<sup>60</sup>, its spin polarization might potentially be affected by the solvents. However, various studies in spintronic devices showed that its interface and spinterface are very robust against mechanical and chemical reaction<sup>2,3,61</sup>. In addition, LSMO has been reported to be a good hole injector in LEDs made by polymers<sup>6,7</sup> and small molecules<sup>62</sup>. Therefore, the different effective spin polarization of between the devices should come from Co/fullerene contact.

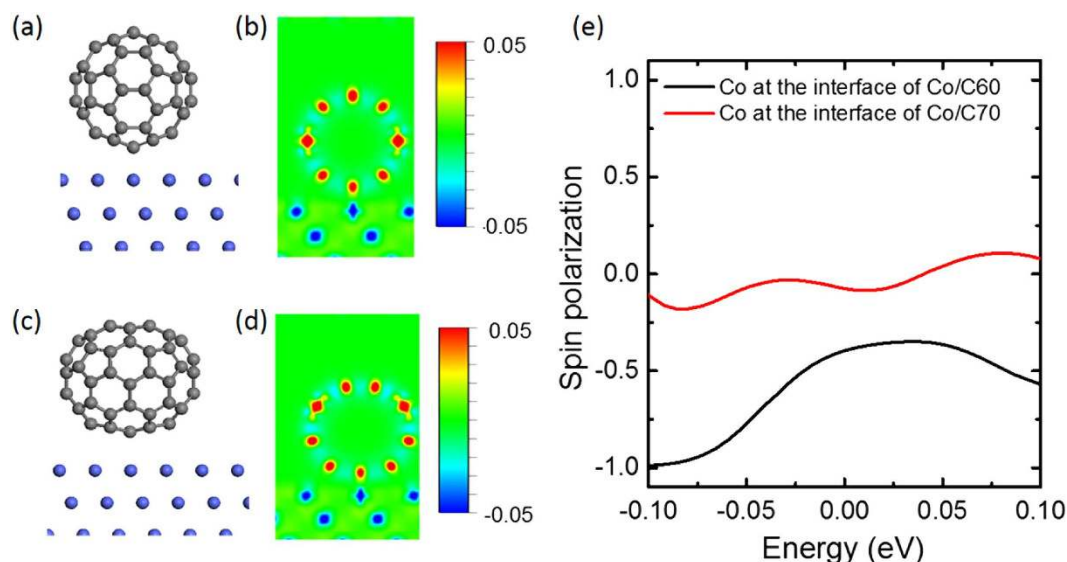


**Figure 5.** (a) Structure and (b) charge density difference isosurfaces of C<sub>60</sub> on Co(111); (c) Structure and (d) charge density difference isosurfaces of C<sub>70</sub> on Co(111). The isovalue is set to  $\pm 0.05 \text{ \AA}^{-3}$ . (e) The spin polarization of the  $dz^2$  orbital electrons of the cobalt contacted with C<sub>70</sub> (red) and red C<sub>60</sub> (black).

## Conclusion

We have successfully fabricated fullerene-based OSVs for studying spin injection into and spin transport through C<sub>60</sub> and C<sub>70</sub> amorphous films. We found that the spin diffusion length in C<sub>70</sub> is considerably longer than that in C<sub>60</sub>. This indicates that its effective SOC and hence curvature SOC is smaller than that in C<sub>60</sub>. This was confirmed by MEL study of fullerene-based LEDs. In addition, the spin diffusion length in the materials is insensitive with temperature. Finally, the effective spin polarization in C<sub>70</sub>-based OSVs was found to be smaller than that in C<sub>60</sub>-based OSVs implying that they have different spinterface effect. This is confirmed by first principle calculation in which the spinterface caused by orbital electron hybridization at the cobalt/C<sub>70</sub> interface is dominant causing smaller effective spin polarization at the interface.

## Methods

The OSVs were fabricated using C<sub>60</sub> or C<sub>70</sub> fullerenes as spacers sandwiched between LSMO (bottom magnetic electrode) and Co (top magnetic electrode). The device scheme is shown as Fig. 1a. LSMO films, having thickness of  $\sim 50 \text{ nm}$  and area of  $5 \times 5 \text{ mm}^2$ , were grown epitaxially on  $\langle 100 \rangle$  oriented SrTiO<sub>3</sub> substrates at  $750^\circ\text{C}$  using magnetron sputtering technique, with Ar and O<sub>2</sub> flux in the ratio of 1:1 in a pressure 4 Pa. The films were subsequently annealed at  $800^\circ\text{C}$  for 2 hours in flowing O<sub>2</sub> atmosphere before slowly cooled to room temperature, the average roughness of LSMO is about 1.0 nm (see Fig. S1(a)). The LSMO films were subsequently patterned using standard photolithography and chemical etching techniques. The LSMO films are already stable against oxidation; they can be cleaned and re-used multiple times without serious degradation. The fullerene spacer was thermally evaporated using an organic evaporation furnace with the evaporation rate of  $0.2 \text{ \AA/s}$  at the base pressure of  $2 \times 10^{-7}$  torr; 15 nm cobalt (capped by 50 nm Al) top electrode was deposited onto the fullerene spacer using a shadow mask. The obtained active device area was typically about  $0.2 \times 0.4 \text{ mm}^2$ . The fabrication of fullerene light emitting diodes was started from patterning indium tin oxide (ITO) electrode, followed by spin-casting of hole transport layer, PEDOT:PSS. The deposition of fullerene and metals were performed in the similar procedure as in OSVs. All the fabrication was done in a nitrogen glove box where the oxygen and water levels are less than 0.1 ppm. Eventually, the OSVs and LEDs were mounted in the cold finger of a closed-cycle refrigerator whose temperature can be varied from 20 to 300 K. The MR was measured using the ‘four probe’ method in the presence of an in-plane magnetic field up to 3 kOe. The electroluminescence of LEDs was detected by a silicon photo diode while sweeping the magnetic field.

In the surface-MOKE method, the beam reflected from the sample passes a Glan-Thompson polarizing beam splitter, where it is separated into two orthogonal polarized beams which are focused by lenses onto diodes A and B of a diode bridge. The light intensities at the diodes,  $I_A$  and  $I_B$ , and the difference signal  $I_{A-B}$  are simultaneously measured using a lock-in amplifier. A polarization balanced bridge detection technique cancels the influence of the background noise. The magnetization of the FM film is proportional to  $I_{A-B}/(I_A + I_B)$ .

## References

1. Naber, W. J. M., Faez, S. & van der Wiel, W. G. Organic spintronics. *J. Phys. D: Appl. Phys.* **40**, R205–R228 (2007).
2. Dediu, V. A., Hueso, L. E., Bergenti, I. & Taliani, C. Spin routes in organic semiconductors. *Nat. Mater.* **8**, 707–716 (2009).
3. Xiong, Z. H., Wu, D., Vardeny, Z. V. & Shi, J. Giant magnetoresistance in organic spin-valves. *Nature* **427**, 821–824 (2004).
4. Majumdar, S., Majumdar, H. S., Laiho, R. & Osterbacka, R. Comparing small molecules and polymer for future organic spin-valves. *J. Alloy. Compd.* **423**, 169–171 (2006).
5. Nguyen, T. D. *et al.* Isotope effect in spin response of  $\pi$ -conjugated polymer films and devices. *Nat. Mater.* **9**, 345–352 (2010).

6. Nguyen, T. D., Ehrenfreund, E. & Vardeny, Z. V. Spin-polarized light-emitting diode based on organic bipolar spin valve. *Science* **337**, 204–209 (2012).
7. Nguyen, T. D., Ehrenfreund, E. & Vardeny, Z. V. The spin-polarized organic light emitting diode. *Synth. Met.* **173**, 16–21 (2013).
8. Bergenti, I. *et al.* Transparent manganite films as hole injectors for organic light emitting diodes. *J. Lumin.* **110**, 384–388 (2004).
9. Nguyen, T. D., Ehrenfreund, E. & Vardeny, Z. V. The development of organic spin valves from unipolar to bipolar operation. *MRS Bulletin* **39**, 585–589 (2014).
10. Datta, S. & Das, B. Electronic analog of the electro-optic modulator. *Appl. Phys. Lett.* **56**, 665–667 (1990).
11. Barraud, C. *et al.* Unravelling the role of the interface for spin injection into organic semiconductors. *Nat. Phys.* **6**, 615–620 (2010).
12. Sanvito, S. Molecular spintronics: the rise of spinterface science. *Nat. Phys.* **6**, 562–564 (2010).
13. Schulz, L. *et al.* Engineering spin propagation across a hybrid organic/inorganic interface using a polar layer. *Nat. Mater.* **10**, 39–44 (2011).
14. Steil, S. *et al.* Spin-dependent trapping of electrons at spinterfaces. *Nat. Phys.* **9**, 242–247 (2013).
15. Djeghloul, F. *et al.* Direct observation of a highly spin-polarized organic spinterface at room temperature. *Sci. Rep.* **3**, 1272 (2013).
16. Schwöbel, J. *et al.* Real-space observation of spin-split molecular orbitals of adsorbed single-molecule magnets. *Nat. Comm.* **3**, 953 (2012).
17. Çakır, D., Otálvaro, D. M. & Brocks, G. From spin-polarized interfaces to giant magnetoresistance in organic spin valves. *Phys. Rev. B* **89**, 115407 (2014).
18. Boehme, C. & Lupton, J. M. An organic response. *Nat. Nano.* **8**, 612–615 (2013).
19. Drew, A. J. *et al.* Direct measurement of the electronic spin diffusion length in a fully functional organic spin valve by low-energy muon spin rotation. *Nat. Mater.* **8**, 109–114 (2009).
20. Jiang, S. W. *et al.* Exchange-dominated pure spin current transport in Alq<sub>3</sub> molecules. *Phys. Rev. Lett.* **115**, 086601 (2015).
21. Kawasugi, Y., Ujino, T. & Tada, H. Room-temperature magnetoresistance in organic spin-valves based on a Co<sub>2</sub>MnSi Heusler alloy. *Org. Electron.* **14**, 3186–3189 (2013).
22. Bobbert, P. A., Wagemans, W., van Oost, F. W. A., Koopmans, B. & Wohlgenannt, M. Theory for spin diffusion in disordered organic semiconductors. *Phys. Rev. Lett.* **102**, 156604 (2009).
23. Yu, Z. G., Ding, F. & Wang, H. Hyperfine interaction and its effects on spin dynamics in organic solids. *Phys. Rev. B* **87**, 205446 (2013).
24. Ando, K., Watanabe, S., Mooser, S., Saitoh, E. & Sirringhaus, H. Solution-processed organic spin-charge converter. *Nat. Mater.* **12**, 622–627 (2013).
25. Watanabe, S. *et al.* Polaron spin current transport in organic semiconductors. *Nat. Phys.* **10**, 308–313 (2014).
26. Koopmans, B. Organic spintronics: pumping spins through polymers. *Nat. Phys.* **10**, 249–250 (2014).
27. Nuccio, L. *et al.* Importance of spin-orbit interaction for the electron spin relaxation in organic semiconductors. *Phys. Rev. Lett.* **110**, 216602 (2013).
28. Wang, F. & Vardeny, Z. V. Recent advances in organic spin-valve devices. *Synth. Met.* **160**, 210–215 (2010).
29. Lin, R. *et al.* Organic spin-valves based on fullerene C<sub>60</sub>. *Synth. Met.* **161**, 553–557 (2011).
30. Zhang, X. *et al.* Observation of a large spin-dependent transport length in organic spin valves at room temperature. *Nat. Commun.* **4**, 1392 (2013).
31. Gobbi, M., Golmar, F., Llopis, R., Casanova, F. & Hueso, L. E. Room-temperature spin transport in C<sub>60</sub>-based spin valves. *Adv. Mater.* **23**, 1609–1613 (2013).
32. Tran, T. L. A., Le, T. Q., Sanderink, J. G. M., van der Wiel, W. G. & de Jong, M. P. The multistep tunneling analogue of conductivity mismatch in organic spin valves. *Adv. Funct. Mater.* **22**, 1180–1189 (2012).
33. Nguyen, T. D., Wang, F., Li, X. G., Ehrenfreund, E. & Vardeny, Z. V. Spin diffusion in fullerene-based devices: morphology effect. *Phys. Rev. B* **87**, 075205 (2013).
34. Huertas-Hernando, D., Guinea, F. & Brataas, A. Spin-orbit coupling in curved graphene, fullerene, nanotubes, and nanotube caps. *Phys. Rev. B* **74**, 155426 (2006).
35. Gobbi, M. *et al.* C<sub>60</sub>/NiFe combination as a promising platform for molecular spintronics. *Org. Electron.* **13**, 366–372 (2012).
36. Steele, G. A. *et al.* Large spin-orbit coupling in carbon nanotubes. *Nat. Commun.* **4**, 1573 (2013).
37. Kuemmeth, F., Ilani, S., Ralph, D. C. & McEuen, P. L. Coupling of spin and orbital motion of electrons in carbon nanotubes. *Nature* **452**, 448–452 (2008).
38. Min, H. *et al.* Intrinsic and Rashba spin-orbit interactions in graphene sheets. *Phys. Rev. B* **74**, 165310 (2006).
39. Arbogast, J. W. & Foote, C. S. Photophysical properties of C<sub>70</sub>. *J. Am. Chem. Soc.* **113**, 8886–8889 (1991).
40. Poluektov, O. G. *et al.* Spin signatures of photogenerated radical anions in polymer-[70] fullerene bulk heterojunctions: high frequency EPR spectroscopy. *J. Phys. Chem. B* **114**, 14426–14429 (2010).
41. Morton, J. R., Preston, K. F. & Negri, F. The EPR spectra of FC<sub>60</sub> and FC<sub>70</sub>. *Chem. Phys. Lett.* **221**, 59–64 (1994).
42. Johnson, R. C., Merrifield, R. E., Avakian, P. & Flippen, R. B. Effects of magnetic fields on the mutual annihilation of triplet excitons in molecular crystals. *Phys. Rev. Lett.* **19**, 285–287 (1967).
43. Frankovich, E. L. *et al.* Magnetic field effects on photoluminescence in PPP. Investigation of the influence of chain length and degree of order. *Chem. Phys. Lett.* **261**, 545–550 (1996).
44. Kroto, H. W., Heath, J. R., O'Brien, S. C., Curl, R. F. & Smalley, R. E. C<sub>60</sub>: buckminsterfullerene. *Nature* **318**, 162–163 (1985).
45. McKenzie, D. R., Davis, C. A., Cockayne, D. J. H., Muller, D. A. & Vassallo, A. M. The structure of the C<sub>70</sub> molecule. *Nature* **355**, 622–624 (1992).
46. Wu, D., Xiong, Z. H., Li, X. G., Vardeny, Z. V. & Shi, J. Magnetic-field-dependent carrier injection at La<sub>2/3</sub>Sr<sub>1/3</sub>MnO<sub>3</sub> and organic semiconductors interfaces. *Phys. Rev. Lett.* **95**, 016802 (2005).
47. Gil, W., Görlitz, D., Horisberger, M. & Kötzler, J. Magnetoresistance anisotropy of polycrystalline cobalt films: geometrical-size and domain effects. *Phys. Rev. B* **72**, 134401 (2005).
48. Jiang, S. W. *et al.* Strong asymmetrical bias dependence of magnetoresistance in organic spin valves: the role of ferromagnetic/organic interfaces. *New J. Phys.* **16**, 013028 (2014).
49. De Teresa, J. M. *et al.* Inverse tunnel magnetoresistance in Co/SrTiO<sub>3</sub>/La<sub>0.7</sub>Sr<sub>0.3</sub>MnO<sub>3</sub>: new ideas on spin-polarized tunneling. *Phys. Rev. Lett.* **82**, 4288–4291 (1999).
50. Zhang, J. & White, R. M. Voltage dependence of magnetoresistance in spin dependent tunneling junctions. *J. Appl. Phys.* **83**, 6512–6514 (1998).
51. Wang, F. & Vardeny, Z. V. Organic spin valves: the first organic spintronics devices. *J. of Mater. Chem.* **19**, 1685–1690 (2009).
52. Haddock, J. N., Zhang, X., Domercq, B. & Kippelen, B. Fullerene based n-typed organic thin-film transistors. *Org. Electron.* **6**, 182–187 (2005).
53. Yu, Z. G. Spin-orbit coupling, spin relaxation, and spin diffusion in organic solids. *Phys. Rev. Lett.* **106**, 106602 (2011).
54. Gimzewski, J. K., Modesti, S., David, T. & Schlittler, R. R. Scanning tunneling microscopy of ordered C<sub>60</sub> and C<sub>70</sub> layers on Au(111), Cu(111), Ag(110), and Au(110) surfaces. *J. Vac. Sci. Technol. B* **12**, 1942–1946 (1994).
55. Sachidanandam, R., Lubensky, T. C. & Harris, A. B. Phenomenological dynamics of C<sub>70</sub>. *Phys. Rev. B* **51**, 12380–12397 (1995).
56. Heiney, P. A. *et al.* Orientational ordering transition in solid C<sub>60</sub>. *Phys. Rev. Lett.* **66**, 2911–2914 (1991).
57. Grünwald, M. *et al.* Vertical organic spin valves in perpendicular magnetic fields. *Phys. Rev. B* **88**, 085319 (2013).
58. Riminucci, A. *et al.* Hanle effect missing in a prototypical organic spintronic device. *Appl. Phys. Lett.* **102**, 092407 (2013).



59. Ehrenfreund, E. & Vardeny, Z. V. Effects of magnetic field on conductance and electroluminescence in organic devices. *Isr. J. Chem* **52**, 552–562 (2012).
60. Li, F. *et al.* Modified Surface Electronic and Magnetic Properties of  $\text{La}_{0.6}\text{Sr}_{0.4}\text{MnO}_3$  Thin Films for Spintronics Applications. *J. Phys. Chem. C* **115**, 16947–16953 (2011).
61. Garcia, V. *et al.* Ferroelectric Control of Spin Polarization. *Science* **327**, 1106–1110 (2010).
62. Bergenti, I. *et al.* Spin polarised electrodes for organic light emitting diodes. *Org. Electron.* **5**, 309–314 (2004).

## Acknowledgements

We acknowledge useful discussion with Profs. Hung Diep, Vally Vardeny and Huong Phan. We thank Mr. Pradip Basnet for helping us with the XRD spectra. This work was supported by University of Georgia start-up funds and the Faculty Research Grant (T.N.), MOST (Contract Nos. 2010CB934401 and 2011YQ120053) and NSFC (Contract No.11434014)(X.F.H.) NSFC and NBRPC (Contract Nos. 2012CB922003, X.G.L.).

## Author Contributions

S.L., R.G. and R.C.S. were responsible for MOKE measurements, the OLED and OSV device fabrication and measurements; B.Y., X.H. and S.L. were responsible for DFT calculation; W.Z. and X.G.L. were responsible for growing and characterizing the LSMO substrates; T.D.N. was responsible for project planning, group managing, and first draft writing.

## Additional Information

**Supplementary information** accompanies this paper at <http://www.nature.com/srep>

**Competing financial interests:** The authors declare no competing financial interests.

**How to cite this article:** Liang, S. *et al.* Curvature-enhanced Spin-orbit Coupling and Spininterface Effect in Fullerene-based Spin Valves. *Sci. Rep.* **6**, 19461; doi: 10.1038/srep19461 (2016).



This work is licensed under a Creative Commons Attribution 4.0 International License. The images or other third party material in this article are included in the article's Creative Commons license, unless indicated otherwise in the credit line; if the material is not included under the Creative Commons license, users will need to obtain permission from the license holder to reproduce the material. To view a copy of this license, visit <http://creativecommons.org/licenses/by/4.0/>